

FABind+: Enhancing Molecular Docking through Improved Pocket Prediction and Pose Generation

Kaiyuan Gao^{1*} Qizhi Pei^{2*} Jinhua Zhu³ Tao Qin⁴ Kun He¹ Tie-Yan Liu⁴ Lijun Wu^{4†}

Abstract

Molecular docking is a pivotal process in drug discovery. While traditional techniques rely on extensive sampling and simulation governed by physical principles, these methods are often slow and costly. The advent of deep learning-based approaches has shown significant promise, offering increases in both accuracy and efficiency. Building upon the foundational work of FABind, a model designed with a focus on speed and accuracy, we present FABind+, an enhanced iteration that largely boosts the performance of its predecessor. We identify pocket prediction as a critical bottleneck in molecular docking and propose a novel methodology that significantly refines pocket prediction, thereby streamlining the docking process. Furthermore, we introduce modifications to the docking module to enhance its pose generation capabilities. In an effort to bridge the gap with conventional sampling/generative methods, we incorporate a simple yet effective sampling technique coupled with a confidence model, requiring only minor adjustments to the regression framework of FABind. Experimental results and analysis reveal that FABind+ remarkably outperforms the original FABind, achieves competitive state-of-the-art performance, and delivers insightful modeling strategies. This demonstrates FABind+ represents a substantial step forward in molecular docking and drug discovery. Our code is in [this URL](https://github.com/lijunwu/FABind-Plus).

1. Introduction

Molecular docking is a foundational technique in drug discovery (Morris et al., 1996; Morris & Lim-Wilby, 2008; Thomsen & Christensen, 2006; AI4Science & Quantum, 2023), serving as a computational strategy to predict the preferred orientation of ligands when bound to a protein target. This predictive process is crucial for the identification and optimization of compounds with therapeutic potential. Traditional methodologies (Friesner et al., 2004; Trott & Olson, 2010; Morris et al., 1996; Verdonk et al., 2003) heavily rely on exhaustive sampling and simulation techniques, which are rooted in the principles of physics and chemistry (Shoichet & Kuntz, 1993; Bernacki et al., 2005; Perez et al., 2016; Huang & Jacobson, 2007). These approaches aim to mimic the complex interactions between ligands and their protein receptors to forecast optimal conformations. Despite their extensive application, the classical methods are often criticized for their computational intensity, which translates into slow processing and significant resource consumption (Pagadala et al., 2017; Huang et al., 2006).

With the rise of computational power and machine learning, deep learning approaches for molecular docking have emerged (Zhang et al., 2023a; Lu et al., 2023; Zhou et al., 2023). These methods leverage neural networks and advanced algorithms to analyze biochemical data. Deep learning methods are categorized as generative models that sample candidates selected by confidence models (Corso et al., 2023b; Wang et al., 2023; Guo et al., 2023), similar to traditional methods, or regression approaches that directly predict coordinates (Stärk et al., 2022; Zhang et al., 2022) or distance matrices followed by coordinate recovery (Masters et al., 2022; Lu et al., 2022). Deep learning promises gains in docking accuracy and efficiency. Notably, FABind (Pei et al., 2023) specifically accelerates docking while maintaining prediction precision.

Despite advances by FABind in rapid regression-based prediction, its accuracy was observed to be not fully aligned with the latest progress (Corso et al., 2023b; Liu et al., 2023; Yan et al., 2023). Here, we introduce FABind+, which features enhanced pocket prediction capabilities and high-quality pose generation. Our first analysis highlights pocket prediction as a pivotal factor, where inaccuracies disrupt the

*Equal contribution ¹School of Computer Science and Technology, Huazhong University of Science and Technology ²Gaoling School of Artificial Intelligence, Renmin University of China ³School of Information Science and Technology, University of Science and Technology of China ⁴Microsoft Research AI4Science. Correspondence to: Lijun Wu <lijunwu@microsoft.com>.

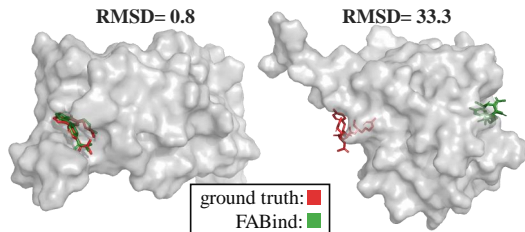


Figure 1. Cases of the predicted docking results. *Left*: a good case with correct pocket and docking pose prediction. *Right*: a bad case that the predicted pocket is far away from the ground truth pocket so to a large RMSD score with incorrect ligand pose.

docking process. As shown in Figure 1, the incorrect pocket from FABind leads to a large root-mean-square deviation (RMSD) score, with 16.25% of pose predicted by FABind having an RMSD greater than 10Å. Obviously, this issue can be attributed to incorrect pocket prediction. To address this, we propose dynamically predicting the pocket radius instead of using a fixed-size sphere, thereby allowing the enlarged pocket to cover the entire potential ligand structure for accurate docking pose prediction. By inheriting the pocket prediction task from FABind, we aim to create a more suitable region for docking by meticulously tuning the multitask framework. For the docking module, we also implement strategies to improve performance. Drawing inspiration from molecular conformation generation methods (Zhu et al., 2022), which underscores the importance of permutation invariance for symmetric atoms, we introduce a permutation loss function to enhance the robustness of the conformation prediction.

As demonstrated by Corso et al. (2023a;b), a sampling model is essential for capturing multiple binding sites and conformations. Therefore, after applying the above enhancement to build a regression-based FABind+, we further exploit its sampling potential. Unlike previous sampling-based methods of training a generative model for capturing multiple conformations, we directly transform the trained regression-based FABind+ into a sampling-based model. Specifically, to address the issue of multiple binding sites, we employ a clustering method to identify all potential pocket candidates, leveraging our residue-level probability for pocket presence. Moreover, we integrate a robust yet simple sampling mechanism based on dropout (Srivastava et al., 2014) to enable FABind+ to sample multiple conformations effectively. Finally, a lightweight confidence model is trained to rank the best-sampled structures.

For evaluation, we conduct comprehensive experiments and analyses on the widely recognized PDDBind v2020 benchmarks (Liu et al., 2017) under various settings. As a regression-based model, FABind+ outperforms all previ-

ous methods with remarkable inference speed. Moreover, by activating the sampling mode, FABind+ is capable of generating diverse and high-quality conformations, thereby further enhancing performance beyond that of the purely regression-based model.

2. Related Work

2.1. Pocket/Binding Site Prediction

Pocket prediction plays an important role in structure-based drug discovery. Early computational methods relied on hand-crafted features, using different modeling approaches such as physical chemical-based, geometric-based, and machine learning-based methods (Stank et al., 2016; Weisel et al., 2007; Capra et al., 2009). For example, sequence-based techniques exploited protein sequences (Taherzadeh et al., 2016; Chen & Jeong, 2009), while structure-based tools examined 3D structures (Le Guilloux et al., 2009; Laskowski, 1995), and the integration of both sequence and 3D structures (Capra et al., 2009). Recently, deep learning has achieved significant advances. Pioneering works applied convolutional neural networks (CNNs) to learn spatial patterns from protein structures (VIART et al., 2020; Pu et al., 2019). DeepSite (Jiménez et al., 2017) and DeepPocket (Gentile et al., 2020) both apply to the sequence profiles of the protein to predict the binding hotspots. Other works includes (Zhang et al., 2019; Ragoza et al., 2017; Zhang et al., 2023b). Among them, Fpocket (Le Guilloux et al., 2009) and P2rank (Krivák & Hoksza, 2018) are two representative works that open-sourced and have been widely adopted in existing works. In this work, we carefully build a dynamic pocket prediction module and integrate this module into the entire molecular docking framework.

2.2. Molecular Docking

Molecular docking, also known as protein-ligand docking, aims to predict the correct binding pose of the protein-ligand complex. Traditional methods typically use physics-informed energy functions to score, rank, and refine the ligand structures, such as AutoDock Vina (Trott & Olson, 2010), SMINA (Koes et al., 2013), GLIDE (Friesner et al., 2004), and GOLD (Jones et al., 1997). Geometric deep learning has been attractive and promising for docking prediction. These methods can be divided into two categories: 1) Regression-based methods that aim to directly predict the docked ligand pose coordinates or optimize the structures with predicted pairwise distances between atoms, such as EquiBind (Stärk et al., 2022), TankBind (Lu et al., 2022), E3Bind (Zhang et al., 2022), and KarmaDock (Zhang et al., 2023a). These methods usually demonstrate clear advantages in inference speed. 2) Sampling-based methods that require multiple ligand poses sampling and then perform optimization or selection among sampled conformation can-

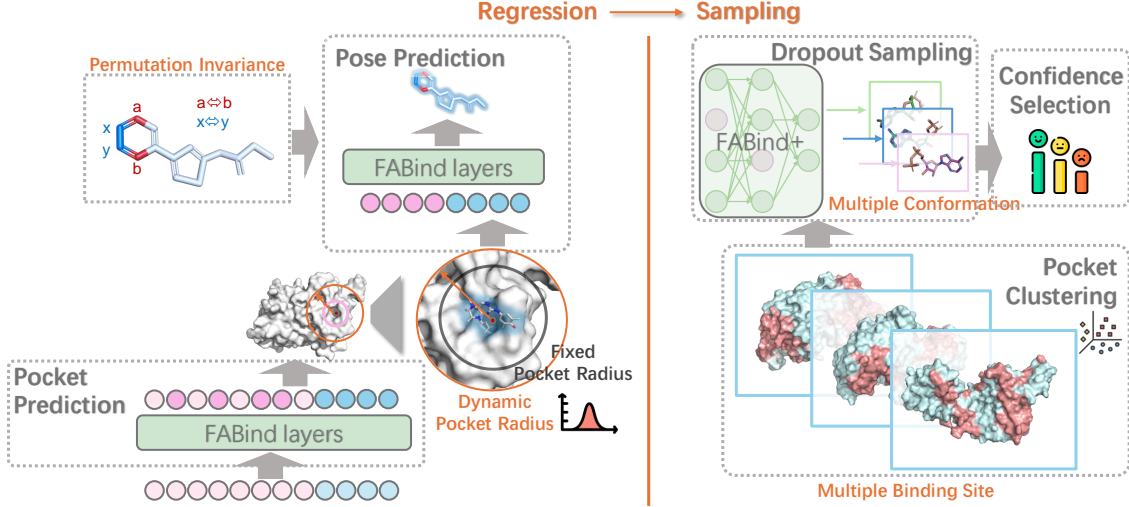


Figure 2. Overall framework of FABind+. *Left:* The regression-based FABind+ consists of the original FABind design and the newly proposed dynamic pocket radius prediction and permutation loss module. *Right:* The sampling version of FABind+, which contains a pocket clustering module, a conformation sampling module, and a confidence selection module.

dicates (Nakata et al., 2023; Corso et al., 2023b; Wang et al., 2023; Guo et al., 2023). While more computationally expensive, sampling-based methods often yield more accurate predictions. FABind (Pei et al., 2023) is a docking framework that is designed to be both efficient and effective. Our work follows FABind to eliminate its limitations and boost its performance. Notably, AlphaFold-latest (Deepmind & Labs, 2023) achieves huge breakthroughs, but in close-form introduction without details. DeltaDock (Yan et al., 2023) and HelixDock (Liu et al., 2023) also obtain competitive results for us. However, they either generate large-scale data with simulators or add external high quality data for the training, which is not a fair comparison.

3. Method

3.1. Preliminaries

Problem Definition. Let $\mathcal{G} = (\mathcal{V} := \{\mathcal{V}^l, \mathcal{V}^p\}, \mathcal{E} := \{\mathcal{E}^l, \mathcal{E}^p, \mathcal{E}^{lp}\})$ denote a protein-ligand complex, where $\mathcal{G}^l = (\mathcal{V}^l, \mathcal{E}^l)$ and $\mathcal{G}^p = (\mathcal{V}^p, \mathcal{E}^p)$ are ligand and protein graph, respectively. The symbols \mathcal{V} and \mathcal{E} represent collections of atoms (residue for protein) and bonds. \mathcal{E}^{lp} in \mathcal{E} is the edge collection between protein and ligand graph. Each node $v = (\mathbf{h}, \mathbf{x}) \in \mathcal{V}$ contains a feature vector \mathbf{h} and its coordinates $\mathbf{x} \in \mathbb{R}^3$. For clarity, $v_i = (\mathbf{h}_i, \mathbf{x}_i) \in \mathcal{V}^l$ is used to denote ligand atom and $v_j = (\mathbf{h}_j, \mathbf{x}_j) \in \mathcal{V}^p$ for protein residue. We use $\mathcal{R}^l \in \mathbb{R}^{|\mathcal{V}^l| \times 3}$ and $\mathcal{R}^p \in \mathbb{R}^{|\mathcal{V}^p| \times 3}$ to represent the conformation of ligand and protein. Given a protein in its bound state and a flexible ligand, our objective is to learn a mapping from the random initialized ligand pose to the bounded conformation $\mathcal{R}^l = \{\mathbf{x}_i\}_{1 \leq i \leq |\mathcal{V}^l|}$. Notably,

we focus on the blind docking setting, where we possess no information regarding the binding pocket.

Background of FABind. FABind (Pei et al., 2023) is a novel deep learning framework that aims to provide both fast and accurate protein-ligand binding structure prediction in an end-to-end manner, which tries to overcome the low efficiency of sampling methods and also the inaccuracy of regression methods. The core innovation in FABind is its unique layer design called “FABind layer” (F). Each FABind layer (l) takes in protein-ligand complex graph and protein-ligand pair embedding and outputs updated embedding and ligand structures:

$$\mathbf{h}_i^{(l+1)}, \mathbf{h}_j^{(l+1)}, \mathbf{x}_i^{(l+1)}, \mathbf{p}_{ij}^{(l+1)} = F(\mathbf{h}_i^{(l)}, \mathbf{h}_j^{(l)}, \mathbf{x}_i^{(l)}, \mathbf{x}_j, \mathbf{p}_{ij}^{(l)}),$$

where $\mathbf{p}_{ij} \in \mathbb{R}^{D \times D}$ is pair embedding for each pair of ligand and protein node and D is hidden size. The FABind layer contains three key components: independent message passing, cross-attention update, and interfacial message passing. The independent message passing captures interactions within the protein and ligand separately, the cross-attention update enhances node representations by exchanging information across the protein and ligand, and the interfacial message passing focuses on modeling interactions at the protein-ligand interface.

Another important technology is how FABind unifies pocket prediction and docking into a unified framework. It introduces a ligand-informed pocket prediction module that utilizes the ligand information to pinpoint the unique binding pocket. This achieves faster and more precise pocket prediction than methods relying on external pocket detectors. The predicted pocket is then leveraged for downstream

docking prediction. Notably, FABind adopts a scheduled sampling (Bengio et al., 2015) training strategy that gradually incorporates the predicted pocket instead of solely using the native pocket, ensuring consistency between training and inference. It also proposes distance map constraints, besides coordinate loss, to refine the predicted pose.

3.2. Enhanced FABind+

Though FABind achieves comparable docking performance with DiffDock (Corso et al., 2023b) in a highly efficient way, it does not show promising advantages (docking accuracy) over existing works (Corso et al., 2023b; Yan et al., 2023). By carefully investigating the evaluations of the predicted docking poses, we find the limitations of FABind can be attributed to both the inaccurate pocket/binding site predictions and the capability of the docking module. Therefore, we propose different techniques to improve both the pocket prediction and the docking modules to enhance final docking. The overall framework of our FABind+ is shown as the left part in Figure 2.

3.2.1. POCKET PREDICTION

Regarding pocket prediction, we found that in FABind, there are many cases where the predicted pocket position is incorrect, as shown in Figure 1. Therefore, we attempt to improve the pocket prediction method here. Specifically, we observed that FABind has proposed effective methods for accurately predicting the pocket center. However, in FABind, the overall pocket is determined by a fixed-radius sphere, which leads to many cases where the predicted pocket is not accurate. If the fixed radius is not large enough, the pocket cannot correctly contain all possible amino acids and atoms of the ligand. Since our docking network requires interactions between all atoms of the ligand and amino acids in the pocket, the size of the pocket being able to contain all atoms of the ligand is very important and can provide a good foundation for the docking module.

To verify the above hypothesis, we plot the max distance between the predicted pocket center (with coordinates \mathbf{x}_o^p) and each ground truth ligand atom (with coordinates \mathbf{x}_i^l , where $1 \leq i \leq |\mathcal{V}^l|$). The max distance, denoted as D_{max} , is formulated as: $D_{max} = \max_{1 \leq i \leq |\mathcal{V}^l|} \|\mathbf{x}_o^p - \mathbf{x}_i^l\|$, where $\|\cdot\|$ represents the Euclidean distance. This max distance is plotted on the x-axis in Figure 3, with the RMSD score between the corresponding predicted ligand pose and ground truth ligand plotted on the y-axis. The analysis shows that cases with larger max distances tend to exhibit larger RMSD errors. And the fixed radius of 20Å in FABind is insufficient to encompass the potential ligand structure. Based on the above analysis and findings, we are motivated to propose our solution: predicting a dynamic pocket radius to cover all atoms of the ligand as much as possible.

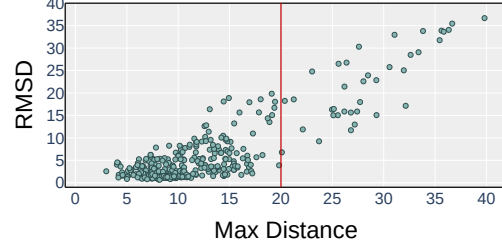


Figure 3. Analysis of pocket prediction and the predicted ligand RMSD. “Max Distance” is the distance between the predicted pocket center and the farthest ground truth ligand atom.

Dynamic Pocket Radius Prediction. To enlarge the pocket coverage with the whole ligand, we propose a dynamic pocket radius prediction module. In the ideal case, even when we predict a wrong pocket center, the radius-enlarged pocket can still cover most of the atoms in the ligand. For this, we simply add a regression head for the pocket radius prediction. The label of the training data is set as the radius of each ground truth ligand conformation, which hence can be viewed as a prediction of the ligand size¹.

Denote the radius of the ground truth ligand conformation as r , with the updated hidden states \mathbf{h}_i for ligand atoms from the pocket prediction module. The radius regression head, represented as ϕ_r , employs a multilayer perceptron (MLP) and the loss function is the Huber loss (Huber, 1992):

$$\hat{r} = \phi_r(\sum_i \mathbf{h}_i), \quad L_r = \text{Huber}(r, \hat{r}). \quad (1)$$

Then, similar to FABind, we calculate the predicted center of the classified residues from the pocket prediction module in FABind and take it as the predicted pocket center, and the circled pocket is then in a sphere near the predicted center under the predicted radius \hat{r} , instead of a fixed radius. In this way, we are able to cover most of the atoms in the ligand for the further docking part.

3.2.2. DOCKING STRUCTURE PREDICTION

Permutation Loss. The rationality of molecular conformation is crucial for the performance of docking procedures. Traditional regression-based methods rely on post-optimization techniques (Stärk et al., 2022; Zhang et al., 2022), which impose constraints on directly predicted conformations to enhance their rationality. However, post-optimization is not only time-consuming but also fails to achieve a fully end-to-end generation of rational conformations. To improve the rationality of generated conformations and reduce dependence on post-optimization, we introduce

¹We also try other choices as training labels, such as the distance between the predicted pocket center and the ground truth pocket center plus the ligand radius. In practice, the ligand radius as label is best for stable training.

the permutation loss (Zhu et al., 2022) to the docking model of FABind+, which is designed to ensure the permutation invariance of symmetric atoms of molecular conformations during training. Denote that the predicted ligand conformation is $\hat{\mathcal{R}}^l$ and the ground truth ligand conformation is \mathcal{R}^l . This loss is defined as:

$$L_p = \min_{\sigma \in \mathbb{S}} \{ \text{Huber}(\mathcal{R}^l, \sigma(\hat{\mathcal{R}}^l)) \}, \quad (2)$$

where \mathbb{S} represents the set of permutation operations applied to symmetric atoms of the molecule. In practice, we use the graph tool² to extract all permutations of a ligand graph. By incorporating permutation loss, the model directly learns to predict more rational molecular structures, streamlining the docking process and enhancing its accuracy.

Enlarge Model Size. To enhance the overall performance of the docking accuracy, we find the capability of the docking module crucial for the final result. Therefore, in this work, we simply enlarge the docking module size. However, since we still aim to maintain the efficiency of the docking speed of FABind, adding more layers will lead to slow inference. For a balance between speed and accuracy, we extend one more FABind layer for docking prediction.

3.3. A Simple Sampling Method

Recently, generative models have been popular in AI research, as well as in the biology, chemistry, and drug discovery fields (Lopez et al., 2020; Bian & Xie, 2021; Cheng et al., 2021). Specific to molecular docking, many works have been proposed to model the docking process in a generative way (Corso et al., 2023b; Wang et al., 2023; Guo et al., 2023). The motivation behind this is to leverage the powerful sampling ability of these generative models, which can sample reasonable docking poses or pockets in the large and extensive search space. To align the line of these sampling-based methods for generative docking, we are interested in extending our FABind+ into a sampling version with minimal modifications (see the right part in Figure 2). Notably, it is obvious that for the sampling-based version, the speed has to be sacrificed, but the accuracy should be ensured and even improved.

3.3.1. SAMPLING METHOD

In DiffDock (Corso et al., 2023b), the authors discussed the problem of the regression model due to the possibility of different pockets in a target protein, which indicates the prediction of different pocket variants is crucial. Hence, in our sampling-based FABind+, we utilize a clustering method for pocket variant prediction. Besides, a simple dropout-based conformation generation method is adopted in our model to produce conformation variants. It is important that

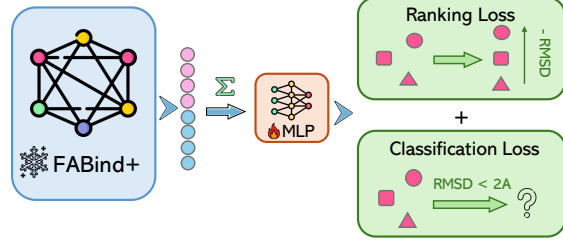


Figure 4. Confidence model training pipeline. We add lightweight MLP layers upon the fixed FABind+ model for the confidence model, which incorporates a ranking loss and a classification loss for training the confidence model.

our modified FABind+ for the sampling version requires no training of the pocket variants and conformation variant generation, which are indeed lightweight and based on the regression-based FABind+.

Clustering for Pocket Variants. The pocket prediction module of FABind is designed to predict a single pocket center, which is insufficient for identifying multiple binding sites. For pocket variants, we adopt the method from (Braun & Fayne, 2022) to use DBSCAN for pocket clustering. This algorithm does not require the pre-specification of cluster centers and exhibits a tolerance for noise, making it a versatile choice among clustering algorithms. During each sampling process, there is a probability p (with $p = 0.5$) that we randomly choose a cluster from the DBSCAN output; otherwise, the initially predicted pocket center is used. The center of this cluster is then adopted as the pocket center. This strategy is aimed at maximizing diversity. Regardless of the method used to determine the pocket center, the radius predicted by the radius prediction module is employed to redefine the pocket boundaries in a spherical manner, ensuring sufficient coverage of potential ligand positions.

Dropout for Conformation Generation. To sample variants of the ligand conformation, we use a very simple trick to do the sampling. Dropout (Srivastava et al., 2014) is a commonly adopted method to overcome overfitting and improve generalization. It randomly drops several units in each model layer and leads to a sub-model over the full model for forward passing. In this work, we utilize the property of randomness from dropout to do the sampling. Since each sub-model produced by dropout is supervised by the ground truth conformation (label) during training, the conformation generated by the sub-model would largely be reasonable and near the correct pose. Therefore, we simply use each forward pass of the sub-model with a dropout to generate the conformation variants. The implementation is also easy, similar to Rdrop (Wu et al., 2021), when generating a size of s conformations for an input ligand x , we can simply repeat the input x for s times in a batch and go through one forward pass to generate s conformations.

²<https://graph-tool.skewed.de>

3.3.2. CONFIDENCE MODEL

After generating multiple conformations as candidates, we need a confidence model to make the final pose selection. In this work, we introduce a lightweight confidence model with only several MLP layers after the docking module. The overall pipeline is shown in Figure 4. Specifically, the hidden states h_i before the structure/coordinates prediction are first summed and then fed into MLP layers for confidence training. During the training phase, the parameters of FABind+ are frozen, allowing for exclusive updates to the parameters of the confidence model.

We employ two loss functions here for better confidence model training. Firstly, we adopt a classification loss identical to the one used in DiffDock, which aims to predict whether the structure of a conformation w.r.t. the ground truth conformation belongs to $\text{RMSD} < 2\text{\AA}$. Secondly, we introduce a ranking loss that concentrates on the relative positions between conformation candidates. We use a pairwise ranking loss that is the same as the reward model training in InstructGPT (Ouyang et al., 2022). Intuitively, for the conformation with a lower RMSD score, we will rank it in front of the one with a larger RMSD. These two losses have different goals, and we find they both contribute to better selection. The details are described in Appendix B.

4. Experiments

4.1. Setting

Data. We evaluate our methods on PDBbind v2020 dataset (Liu et al., 2017), curated from Protein Data Bank (PDB) (Burley et al., 2021). Consistent with the data split method of EquiBind, as adopted in most prior research (Corso et al., 2023b; Stärk et al., 2022; Lu et al., 2022; Pei et al., 2023), we used structures published before 2019 for training and those from 2019 onwards for testing. We excluded proteins with over 1500 residues and ligands with more than 150 atoms, resulting in 17,644 samples for training, 958 for validation, and 363 for testing. Further details about our preprocessing steps are outlined in Appendix Section A.1.

Baselines. FABind+ is benchmarked against many traditional methods and deep learning models. QVINA-W, GINA (McNutt et al., 2021), SMINA (Koes et al., 2013), GLIDE (Friesner et al., 2004) and VINA (Trott & Olson, 2010) are concluded as the powerful traditional methods. Deep learning models can be categorized into two main classes: sampling-based and regression-based models. For the sampling-based models, we include DiffDock (Corso et al., 2023b), and for regression-based models, we include EquiBind (Stärk et al., 2022) TankBind (Lu et al., 2022), E3Bind (Zhang et al., 2022), and FABind (Pei et al., 2023).

Evaluation Metrics. Our evaluation employs two key metrics: (1) *Ligand RMSD*: This metric measures the root-mean-square deviation (RMSD) between the predicted and ground-truth ligand coordinates. We report the symmetry-corrected RMSD using sPyRMSD³ (Meli & Biggin, 2020). Detailed descriptions can be found in Appendix Section A.2. (2) *Centroid Distance*: This metric calculates the Euclidean distance between the centroids of the predicted and true ligand structures. It reflects binding site prediction accuracy.

Implementation Details. Initial ligand conformations are generated using the ETKDG algorithm (Riniker & Landrum, 2015), followed by MMFF optimization via RDKit (Landrum et al., 2013), which produces the random generation of a low-energy ligand conformation. For pocket radius prediction, considering the fixed radius of FABind is 20 \AA , we adjust any predicted radius falling below this 20 \AA threshold to 20 \AA . This adjustment ensures the predicted pocket is at least as large as those predicted by FABind. For other hyperparameters and training configurations, we put the details in Appendix C.

4.2. Main results

Blind Self-Docking Performance. Blind self-docking is the process of docking a flexible ligand to a protein without knowing the exact binding site, requiring accurate predictions of the translation, rotation, and conformation of the ligand. From the results in Table 1, our regression-based approach significantly advances the performance over the previous state-of-the-art, DiffDock. It achieves a success rate of 43.5% for ligand atomic RMSD less than 2 \AA , surpassing DiffDock by 5 percentage points. This model demonstrates superior accuracy across the board, as evidenced by improvements in both the mean RMSD and the percentage of predictions under 2 \AA and 5 \AA .

On the other hand, our sampling-based model shows exceptional results, especially as the sample size increases. With a sample size of 10, it performs slightly better than the regression-based model. As we expand the sample size to 40, mirroring the setting used by DiffDock, our sampling-based model delivers superior performance across most metrics. Notably, while the accuracy of highly precise predictions ($\text{RMSD} < 2\text{\AA}$) is slightly improved (43.8%), it significantly improves the prediction of more challenging targets, as indicated by an improved 75th percentile. This advancement may be credited to the implementation of clustering for multiple binding sites, which aids in correcting predictions with incorrect pocket identification.

Blind Self-Docking Performance for Unseen Proteins. In this section we seek to assess the generalization capability of FABind+ on proteins not encountered during the training

³<https://github.com/RMeli/spyrmsd>

Table 1. Performance of flexible blind self-docking. The number of poses that DiffDock and FABind+ sample is specified in parentheses. FABind+ without parentheses denotes regression-based performance. Methods operating solely on the CPU are marked with “*”. All baseline results (with the exception of those from DiffDock, as reported in their paper) are sourced from Pei et al. (2023). The best results are highlighted in **bold**, and the second-best scores are marked with an underline.

Methods	Ligand RMSD								Centroid Distance								Runtime (s)	
	Percentiles ↓				% Below ↑				Percentiles ↓				% Below ↑					
	25%	50%	75%	Mean	2Å	5Å	25%	50%	75%	Mean	2Å	5Å	25%	50%	75%	Mean		
<i>traditional docking softwares</i>																		
QVINA-W	2.5	7.7	23.7	13.6	20.9	40.2	0.9	3.7	22.9	11.9	41.0	54.6	49*					
GNINA	2.8	8.7	22.1	13.3	21.2	37.1	1.0	4.5	21.2	11.5	36.0	52.0	146					
SMINA	3.8	8.1	17.9	12.1	13.5	33.9	1.3	3.7	16.2	9.8	38.0	55.9	146*					
GLIDE	2.6	9.3	28.1	16.2	21.8	33.6	0.8	5.6	26.9	14.4	36.1	48.7	1405*					
VINA	5.7	10.7	21.4	14.7	5.5	21.2	1.9	6.2	20.1	12.1	26.5	47.1	205*					
<i>deep learning-based methods</i>																		
EQUIBIND	3.8	6.2	10.3	8.2	5.5	39.1	1.3	2.6	7.4	5.6	40.0	67.5	0.03					
TANKBIND	2.6	4.2	7.6	7.8	17.6	57.8	0.8	1.7	4.3	5.9	55.0	77.8	0.87					
E3BIND	2.1	3.8	7.8	7.2	23.4	60.0	0.8	1.5	4.0	5.1	60.0	78.8	0.44					
DIFFDOCK (10)	1.5	3.6	7.1	-	35.0	61.7	0.5	1.2	3.3	-	63.1	80.7	20.81					
DIFFDOCK (40)	1.4	3.3	7.3	-	38.2	63.2	0.5	1.2	3.2	-	64.5	80.5	82.83					
FABIND	1.7	3.1	6.7	6.4	33.1	64.2	0.7	1.3	3.6	4.7	60.3	80.2	0.12					
<i>our model</i>																		
FABIND+	1.2	<u>2.6</u>	5.8	<u>5.2</u>	<u>43.5</u>	71.1	0.4	1.0	<u>2.9</u>	3.5	67.5	84.0	0.16					
FABIND+ (10)	1.4	<u>2.6</u>	<u>5.4</u>	5.1	42.1	<u>72.5</u>	0.5	<u>1.1</u>	2.6	3.5	<u>68.3</u>	<u>85.7</u>	1.6					
FABIND+ (40)	1.3	<u>2.4</u>	<u>5.3</u>	5.1	43.8	<u>73.3</u>	0.5	1.0	2.6	3.5	69.1	86.2	6.4					

phase. Following previous works (Zhang et al., 2022; Pei et al., 2023), we evaluate the performance of FABind+ on a set of proteins filtered based on their UniProt IDs, specifically retaining only those samples whose proteins are not seen in the training and validation stages. The results of this evaluation are summarized in Table 2. It is evident from the findings that FABind+ exhibits superior performance, surpassing all baseline methods and its predecessor, FABind, across almost all metrics. This performance underscores the effectiveness of our enhanced design in achieving robust generalization on unseen proteins.

Performance Scaling with Increased Sample Size. To enhance the understanding of the sampling capacity, we depicted “Top1”, “Top5”, “Top10”, and “Perfect Selection” across varying sample sizes in Figure 5. “Perfect selection” denotes the act of selecting the sample with the lowest RMSD. DiffDock stands as a highly powerful generative model, and akin to DiffDock, our approach demonstrates significant performance gains as the sample size increases. When the sample size reaches 40, we are able to dock 51.2% of samples with an RMSD lower than 2Å. Our growth curves for the top1, top5, and top10 selections also exhibit a similar pattern to those of DiffDock, albeit at a slower pace. This deceleration may be attributed to the increased coverage of samples, where the remaining samples are considerably more challenging to dock. However, the observation of similar trends suggests that our lightweight confidence model is equally effective. In contrast to their 20M parameter model,

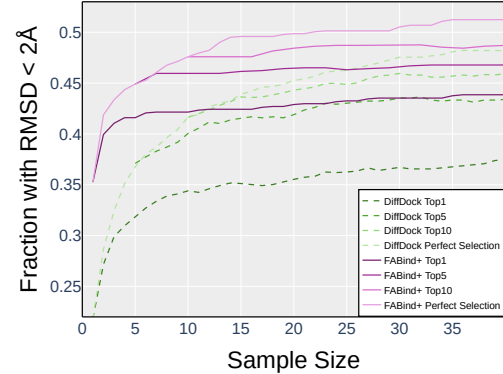


Figure 5. Scaling Curve while Increasing Sample Size.

our model is substantially smaller, with only 6M parameters and based on a simple MLP. Indeed, while our curves outperform those of DiffDock, this advantage begins with our random selection (sample size=1) outperforming DiffDock by about 15%. This does not necessarily indicate that the sampling ability brought forth by dropout or pocket clustering surpasses that of diffusion or other generative methods. However, it does imply that achieving enhanced sampling capacity in docking does not strictly require reliance on generative modeling.

5. Analysis

Pocket Radius Module Analysis. As discussed in Section 3.2.1, we introduce dynamic pocket radius prediction to

Table 2. Performance of flexible blind self-docking on unseen receptors. All baseline results are sourced from Pei et al. (2023).

Methods	Ligand RMSD						Centroid Distance					
	Percentiles ↓				% Below ↑		Percentiles ↓				% Below ↑	
	25%	50%	75%	Mean	2Å	5Å	25%	50%	75%	Mean	2Å	5Å
<i>traditional docking softwares</i>												
QVINA-W	3.4	10.3	28.1	16.9	15.3	31.9	1.3	6.5	26.8	15.2	35.4	47.9
GNINA	4.5	13.4	27.8	16.7	13.9	27.8	2.0	10.1	27.0	15.1	25.7	39.5
SMINA	4.8	10.9	26.0	15.7	9.0	25.7	1.6	6.5	25.7	13.6	29.9	41.7
GLIDE	3.4	18.0	31.4	19.6	19.6	28.7	1.1	17.6	29.1	18.1	29.4	40.6
VINA	7.9	16.6	27.1	18.7	1.4	12.0	2.4	15.7	26.2	16.1	20.4	37.3
<i>deep learning-based methods</i>												
EQUIBIND	5.9	9.1	14.3	11.3	0.7	18.8	2.6	6.3	12.9	8.9	16.7	43.8
TANKBIND	3.4	5.7	10.8	10.5	3.5	43.7	1.2	2.6	8.4	8.2	40.9	70.8
E3BIND	3.0	6.1	10.2	10.1	6.3	38.9	1.2	2.3	7.0	7.6	43.8	66.0
DIFFDOCK (10)	3.2	6.4	16.5	11.8	14.2	38.7	1.1	2.8	13.3	9.3	39.7	62.6
DIFFDOCK (40)	2.8	6.4	16.3	12.0	17.2	42.3	1.0	2.7	14.2	9.8	43.3	62.6
FABIND	2.2	3.4	8.3	7.7	19.4	60.4	0.9	1.5	4.7	5.9	57.6	75.7
<i>our model</i>												
FABIND+	1.6	3.3	8.9	7.0	34.7	63.2	0.5	1.5	4.2	5.1	58.3	77.1
FABIND+(10)	1.7	3.0	8.2	7.5	<u>34.0</u>	<u>63.2</u>	0.8	1.4	4.6	5.7	61.8	76.4
FABIND+(40)	1.7	2.9	8.4	<u>7.2</u>	<u>33.3</u>	63.9	0.8	1.5	4.6	5.4	<u>59.7</u>	77.1

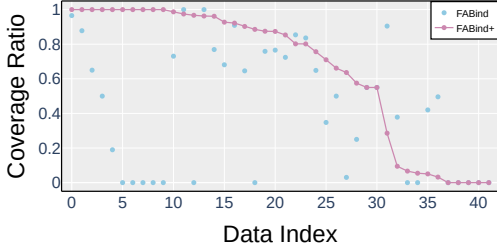


Figure 6. The coverage ratio comparison between FABind (blue) and FABind+ (pink). Samples are sorted in descending order according to the coverage ratio of FABind+, and the corresponding points are connected to facilitate a clear comparison.

make the pocket cover all atoms of the ligand as much as possible. In this section, we further compare the predicted pockets from FABind and FABind+. We focus on the coverage ratio performance within a subset of the test set, defined by the union of test samples where either FABind or FABind+ could not achieve a 100% coverage ratio. The results, as depicted in Figure 6, reveal that within this collective of test samples, FABind+ demonstrates superior performance, with the coverage ratio for the majority of FABind+ predictions being higher than that of FABind. Such outcomes demonstrate the effectiveness of our proposed dynamic pocket radius prediction. Further analysis is reported in Appendix Section D.

Permutation-invariant Loss Analysis. To elucidate the impact of the permutation-invariant loss on the generated conformations, we present two cases in Figure 7 from FABind (without permutation-invariant loss) and FABind+, respectively. Ligands in these cases contain rings that are locally

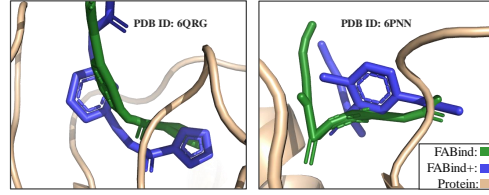


Figure 7. Cases (PDB 6QRG and PDB 6PPN) for permutation-invariant loss analysis. We show the ground truth protein and the predicted conformations by FABind in green and FABind+ in blue.

symmetric. FABind fails to generate the conformations of these rings, with the atoms on the rings being aligned linearly, whereas FABind+ successfully predicts their conformations. This discrepancy arises because the model encounters samples with the same symmetric substructure patterns, such as benzene rings, during training, though the ordering of the atoms may differ. Without the permutation-invariant loss, the model might learn a variety of local optima associated with different atom arrangements. These cases further underscore the significance of permutation-invariant loss in conformation prediction.

Pocket Clustering Analysis. In this section we conduct a case study to show the effectiveness of our pocket clustering method to detect multiple binding sites, as discussed in Section 3.3.1. We select the protein (PDB 6CKL), which is characterized by its symmetric arrangement of two chains. This symmetry results in two ground truth pockets along with their corresponding ligand conformations. As depicted in Figure 8, with our clustering approach, FABind+ successfully identify both pockets and the corresponding docking

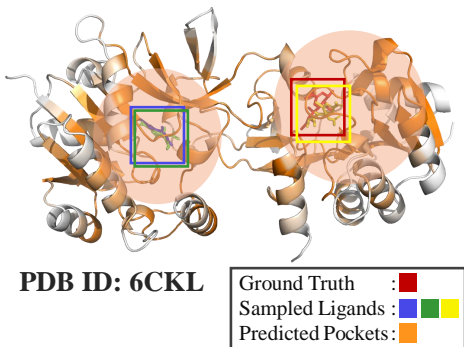


Figure 8. Case for pocket clustering.

conformations through sampling methods. This outcome demonstrates the proficiency of FABind+ in dealing with scenarios involving multiple binding sites, particularly in proteins that form dimers or polymers.

6. Conclusion

In this work, we propose a molecular docking framework FABind+ based on its previous FABind method. The enhanced FABind+ contains a novel dynamic pocket radius prediction and constrained permutation loss for pose generation. Besides, we also extend the FABind+ to be a sampling version using the dropout trick and a light confidence model. Results show that FABind+ largely outperforms the FABind and achieves superior docking performance. In the future, we will continue exploring better model structures for docking and push the result of alphafold-latest.

Impact Statements

This paper presents work whose goal is to advance the field of Machine Learning. There are many potential societal consequences of our work, none which we feel must be specifically highlighted here.

References

AI4Science, M. R. and Quantum, M. A. The impact of large language models on scientific discovery: a preliminary study using gpt-4. *arXiv preprint arXiv:2311.07361*, 2023.

Bengio, S., Vinyals, O., Jaitly, N., and Shazeer, N. Scheduled sampling for sequence prediction with recurrent neural networks. *Advances in neural information processing systems*, 28, 2015.

Bernacki, K., Kalyanaraman, C., and Jacobson, M. P. Virtual ligand screening against escherichia coli dihydrofolate reductase: improving docking enrichment using physics-based methods. *SLAS Discovery*, 10(7):675–681, 2005.

Bian, Y. and Xie, X.-Q. Generative chemistry: drug discovery with deep learning generative models. *Journal of Molecular Modeling*, 27:1–18, 2021.

Braun, J. and Fayne, D. Mapping of protein binding sites using clustering algorithms-development of a pharmacophore based drug discovery tool. *Journal of Molecular Graphics and Modelling*, 115:108228, 2022.

Burley, S. K., Bhikadiya, C., Bi, C., Bittrich, S., Chen, L., Crichlow, G. V., Christie, C. H., Dalenberg, K., Di Costanzo, L., Duarte, J. M., et al. Rcsb protein data bank: powerful new tools for exploring 3d structures of biological macromolecules for basic and applied research and education in fundamental biology, biomedicine, biotechnology, bioengineering and energy sciences. *Nucleic acids research*, 49(D1):D437–D451, 2021.

Capra, J. A., Laskowski, R. A., Thornton, J. M., Singh, M., and Funkhouser, T. A. Predicting protein ligand binding sites by combining evolutionary sequence conservation and 3d structure. *PLoS computational biology*, 5(12):e1000585, 2009.

Chen, X.-w. and Jeong, J. C. Sequence-based prediction of protein interaction sites with an integrative method. *Bioinformatics*, 25(5):585–591, 2009.

Cheng, Y., Gong, Y., Liu, Y., Song, B., and Zou, Q. Molecular design in drug discovery: a comprehensive review of deep generative models. *Briefings in bioinformatics*, 22(6):bbab344, 2021.

Cordella, L. P., Foggia, P., Sansone, C., and Vento, M. A (sub) graph isomorphism algorithm for matching large graphs. *IEEE transactions on pattern analysis and machine intelligence*, 26(10):1367–1372, 2004.

Corso, G., Deng, A., Polizzi, N., Barzilay, R., and Jaakkola, T. The discovery of binding modes requires rethinking docking generalization. In *NeurIPS 2023 Generative AI and Biology (GenBio) Workshop*, 2023a.

Corso, G., Jing, B., Barzilay, R., Jaakkola, T., et al. Diffdock: Diffusion steps, twists, and turns for molecular docking. In *International Conference on Learning Representations (ICLR 2023)*, 2023b.

Deepmind, G. and Labs, I. Performance and structural coverage of the latest, in-development alphafold model. 2023.

Friesner, R. A., Banks, J. L., Murphy, R. B., Halgren, T. A., Klicic, J. J., Mainz, D. T., Repasky, M. P., Knoll, E. H., Shelley, M., Perry, J. K., et al. Glide: a new approach for rapid, accurate docking and scoring. 1. method and assessment of docking accuracy. *Journal of medicinal chemistry*, 47(7):1739–1749, 2004.

Gentile, F., Agrawal, V., Hsing, M., Ton, A.-T., Ban, F., Norinder, U., Gleave, M. E., and Cherkasov, A. Deep docking: a deep learning platform for augmentation of structure based drug discovery. *ACS central science*, 6(6):939–949, 2020.

Guo, H., Liu, S., Mingdi, H., Lou, Y., and Jing, B. Diffdock-site: A novel paradigm for enhanced protein-ligand predictions through binding site identification. In *NeurIPS 2023 Generative AI and Biology (GenBio) Workshop*, 2023.

Huang, N. and Jacobson, M. P. Physics-based methods for studying protein-ligand interactions. *Current Opinion in Drug Discovery and Development*, 10(3):325, 2007.

Huang, N., Kalyanaraman, C., Bernacki, K., and Jacobson, M. P. Molecular mechanics methods for predicting protein-ligand binding. *Physical Chemistry Chemical Physics*, 8(44):5166–5177, 2006.

Huber, P. J. Robust estimation of a location parameter. In *Breakthroughs in statistics: Methodology and distribution*, pp. 492–518. Springer, 1992.

Jiménez, J., Doerr, S., Martínez-Rosell, G., Rose, A. S., and De Fabritiis, G. Deepsite: protein-binding site predictor using 3d-convolutional neural networks. *Bioinformatics*, 33(19):3036–3042, 2017.

Jones, G., Willett, P., Glen, R. C., Leach, A. R., and Taylor, R. Development and validation of a genetic algorithm for flexible docking. *Journal of molecular biology*, 267(3):727–748, 1997.

Kingma, D. P. and Ba, J. Adam: A method for stochastic optimization. *arXiv preprint arXiv:1412.6980*, 2014.

Koes, D. R., Baumgartner, M. P., and Camacho, C. J. Lessons learned in empirical scoring with smina from the csar 2011 benchmarking exercise. *Journal of chemical information and modeling*, 53(8):1893–1904, 2013.

Krivák, R. and Hoksza, D. P2rank: machine learning based tool for rapid and accurate prediction of ligand binding sites from protein structure. *Journal of cheminformatics*, 10:1–12, 2018.

Landrum, G. et al. Rdkit: A software suite for cheminformatics, computational chemistry, and predictive modeling. *Greg Landrum*, 2013.

Laskowski, R. A. Surfnet: a program for visualizing molecular surfaces, cavities, and intermolecular interactions. *Journal of molecular graphics*, 13(5):323–330, 1995.

Le Guilloux, V., Schmidtke, P., and Tuffery, P. Fpocket: an open source platform for ligand pocket detection. *BMC bioinformatics*, 10(1):1–11, 2009.

Liu, L., He, D., Ye, X., Zhang, S., Zhang, X., Zhou, J., Li, J., Chai, H., Wang, F., He, J., et al. Pre-training on large-scale generated docking conformations with helixdock to unlock the potential of protein-ligand structure prediction models. *arXiv preprint arXiv:2310.13913*, 2023.

Liu, Z., Su, M., Han, L., Liu, J., Yang, Q., Li, Y., and Wang, R. Forging the basis for developing protein–ligand interaction scoring functions. *Accounts of chemical research*, 50(2):302–309, 2017.

Lopez, R., Gayoso, A., and Yosef, N. Enhancing scientific discoveries in molecular biology with deep generative models. *Molecular systems biology*, 16(9):e9198, 2020.

Lu, W., Wu, Q., Zhang, J., Rao, J., Li, C., and Zheng, S. Tankbind: Trigonometry-aware neural networks for drug-protein binding structure prediction. *bioRxiv*, 2022.

Lu, W., Zhang, J.-X., Huang, W., Zhang, Z., Jia, X., Wang, Z., Shi, L., Li, C., Wolynes, P., and Zheng, S. Dynamicbind: Predicting ligand-specific protein-ligand complex structure with a deep equivariant generative model. 2023.

Masters, M., Mahmoud, A. H., Wei, Y., and Lill, M. A. Deep learning model for flexible and efficient protein-ligand docking. In *ICLR2022 Machine Learning for Drug Discovery*, 2022. URL <https://openreview.net/forum?id=WNwsnE81meC>.

McNutt, A. T., Francoeur, P., Aggarwal, R., Masuda, T., Meli, R., Ragoza, M., Sunseri, J., and Koes, D. R. Gnina 1.0: molecular docking with deep learning. *Journal of cheminformatics*, 13(1):1–20, 2021.

Meli, R. and Biggin, P. C. spyrmsd: symmetry-corrected rmsd calculations in python. *Journal of Cheminformatics*, 12(1):49, 2020.

Morris, G. M. and Lim-Wilby, M. Molecular docking. *Molecular modeling of proteins*, pp. 365–382, 2008.

Morris, G. M., Goodsell, D. S., Huey, R., and Olson, A. J. Distributed automated docking of flexible ligands to proteins: parallel applications of autodock 2.4. *Journal of computer-aided molecular design*, 10(4):293–304, 1996.

Nakata, S., Mori, Y., and Tanaka, S. End-to-end protein-ligand complex structure generation with diffusion-based generative models. *BMC bioinformatics*, 24(1):1–18, 2023.

Ouyang, L., Wu, J., Jiang, X., Almeida, D., Wainwright, C., Mishkin, P., Zhang, C., Agarwal, S., Slama, K., Ray, A., et al. Training language models to follow instructions with human feedback. *Advances in Neural Information Processing Systems*, 35:27730–27744, 2022.

Pagadala, N. S., Syed, K., and Tuszynski, J. Software for molecular docking: a review. *Biophysical reviews*, 9: 91–102, 2017.

Pei, Q., Gao, K., Wu, L., Zhu, J., Xia, Y., Xie, S., Qin, T., He, K., Liu, T.-Y., and Yan, R. Fabind: Fast and accurate protein-ligand binding. In *Thirty-seventh Conference on Neural Information Processing Systems*, 2023.

Perez, A., Morrone, J. A., Simmerling, C., and Dill, K. A. Advances in free-energy-based simulations of protein folding and ligand binding. *Current opinion in structural biology*, 36:25–31, 2016.

Pu, L., Govindaraj, R. G., Lemoine, J. M., Wu, H.-C., and Brylinski, M. Deepdrug3d: classification of ligand-binding pockets in proteins with a convolutional neural network. *PLoS computational biology*, 15(2):e1006718, 2019.

Ragoza, M., Hochuli, J., Idrobo, E., Sunseri, J., and Koes, D. R. Protein-ligand scoring with convolutional neural networks. *Journal of chemical information and modeling*, 57(4):942–957, 2017.

Riniker, S. and Landrum, G. A. Better informed distance geometry: using what we know to improve conformation generation. *Journal of chemical information and modeling*, 55(12):2562–2574, 2015.

Shoichet, B. K. and Kuntz, I. D. Matching chemistry and shape in molecular docking. *Protein Engineering, Design and Selection*, 6(7):723–732, 1993.

Srivastava, N., Hinton, G., Krizhevsky, A., Sutskever, I., and Salakhutdinov, R. Dropout: a simple way to prevent neural networks from overfitting. *The journal of machine learning research*, 15(1):1929–1958, 2014.

Stank, A., Kokh, D. B., Fuller, J. C., and Wade, R. C. Protein binding pocket dynamics. *Accounts of chemical research*, 49(5):809–815, 2016.

Stärk, H., Ganea, O., Pattanaik, L., Barzilay, R., and Jaakkola, T. Equibind: Geometric deep learning for drug binding structure prediction. In *International Conference on Machine Learning*, pp. 20503–20521. PMLR, 2022.

Taherzadeh, G., Yang, Y., Zhang, T., Liew, A. W.-C., and Zhou, Y. Sequence-based prediction of protein-peptide binding sites using support vector machine. *Journal of computational chemistry*, 37(13):1223–1229, 2016.

Thomsen, R. and Christensen, M. H. Moldock: a new technique for high-accuracy molecular docking. *Journal of medicinal chemistry*, 49(11):3315–3321, 2006.

Trott, O. and Olson, A. J. Autodock vina: improving the speed and accuracy of docking with a new scoring function, efficient optimization, and multithreading. *Journal of computational chemistry*, 31(2):455–461, 2010.

Verdonk, M. L., Cole, J. C., Hartshorn, M. J., Murray, C. W., and Taylor, R. D. Improved protein-ligand docking using gold. *Proteins: Structure, Function, and Bioinformatics*, 52(4):609–623, 2003.

VIART, B. T., Lorenzi, C., Moriel-Carretero, M., and Kos-sida, S. Pickpocket: Pocket binding prediction for specific ligands family using neural networks. *bioRxiv*, pp. 2020–04, 2020.

Wang, Z., Srinivasan, B., Shen, Z., and Karypis, G. Flexidock: Compositional diffusion models for flexible molecular docking. 2023.

Weisel, M., Proschak, E., and Schneider, G. Pocketpicker: analysis of ligand binding-sites with shape descriptors. *Chemistry Central Journal*, 1(1):1–17, 2007.

Wu, L., Li, J., Wang, Y., Meng, Q., Qin, T., Chen, W., Zhang, M., Liu, T.-Y., et al. R-drop: Regularized dropout for neural networks. *Advances in Neural Information Processing Systems*, 34:10890–10905, 2021.

Yan, J., Zhang, Z., Zhang, K., and Liu, Q. Multi-scale iterative refinement towards robust and versatile molecular docking. *arXiv preprint arXiv:2311.18574*, 2023.

Zhang, H., Liao, L., Saravanan, K. M., Yin, P., and Wei, Y. Deepbindrg: a deep learning based method for estimating effective protein-ligand affinity. *PeerJ*, 7:e7362, 2019.

Zhang, X., Zhang, O., Shen, C., Qu, W., Chen, S., Cao, H., Kang, Y., Wang, Z., Wang, E., Zhang, J., et al. Efficient and accurate large library ligand docking with karmadock. *Nature Computational Science*, 3(9):789–804, 2023a.

Zhang, Y., Cai, H., Shi, C., Zhong, B., and Tang, J. E3bind: An end-to-end equivariant network for protein-ligand docking. *arXiv preprint arXiv:2210.06069*, 2022.

Zhang, Y., Huang, W., Wei, Z., Yuan, Y., and Ding, Z. Equipocket: an e (3)-equivariant geometric graph neural network for ligand binding site prediction. *arXiv preprint arXiv:2302.12177*, 2023b.

Zhou, G., Gao, Z., Ding, Q., Zheng, H., Xu, H., Wei, Z., Zhang, L., and Ke, G. Uni-mol: a universal 3d molecular representation learning framework. 2023.

Zhu, J., Xia, Y., Liu, C., Wu, L., Xie, S., Wang, Y., Wang, T., Qin, T., Zhou, W., Li, H., Liu, H., and Liu, T. Direct molecular conformation generation. *Trans. Mach. Learn. Res.*, 2022, 2022. URL <https://openreview.net/forum?id=1CPOHiztuw>.

A. Experiment Details

A.1. Dataset Processing

We keep the dataset split consistent with previous works (Lu et al., 2022; Guo et al., 2023; Pei et al., 2023). The selected 968 validation structures are from data before 2019, and 363 test structures are from 2019 onwards, both ensuring no ligand overlap with the training set. For the training set, we filter out a few samples that could not be read by RDKit or TorchDrug⁴, leaving 17,795 complexes. We retain protein chains with the nearest atom of the small molecule within 10 Å. Subsequently, samples with protein chains longer than 1500 amino acids, molecules larger than 150 atoms, or inadequate contact (less than 5 amino acids within 10 Å of molecule atoms) were excluded. These criteria resulted in the exclusion of 118, 32, and 1 sample, successively, ultimately yielding 17,644 samples for training.

A.2. Symmetry-Corrected RMSD

In the reported results, the root-mean-square deviation (RMSD) is calculated using sPyRMSD (Meli & Biggin, 2020). sPyRMSD utilizes a graph matching tool to identify all possible graph isomorphisms, returning the minimum RMSD. This process is aligned with our permutation loss computation. This approach is consistent with our computation of permutation loss. In practice, given the limited number of isomorphic molecules in the test set, we observe a negligible performance gain compared to standard RMSD calculations.

A.3. Permutation Loss Implementation

We utilize the graph-tool toolkit⁵ to identify all symmetric atoms following previous work (Zhu et al., 2022). According to sPyRMSD (Meli & Biggin, 2020), both graph-tool and networkx⁶ are capable of extracting all permutations. Specifically, an isomorphism between graphs A and B is a bijective mapping of the vertices of graph A to vertices of graph B that preserves the edge structure of the graphs (molecular connectivity in the case of molecular graphs). The problem of finding symmetric atoms can be converted to a graph isomorphism problem.

The implementation of graph-tool is based on VF2 algorithm (Cordella et al., 2004). In FABind+, the identification of symmetric atoms is performed offline with multi-processing. This preprocessing takes a few hours to extract all possible permutations of the PDBBind dataset, which is relatively short compared to the training time. Also, it will not increase training cost since the average number of permutations on our used dataset is only 10.1. The detailed statistics is in Table 3.

Table 3. Statistics on the number of permutations.

No. Permutation	≤ 2	≤ 4	≤ 8	≤ 16	≤ 32	≤ 64	≤ 128
Percentage	58.8%	75.9%	87.7%	94.5%	97.7%	98.8%	99.4%

B. Loss Design of Confidence Model

The training objective includes both classification loss, denoted as L_{cls} , and ranking loss, denoted as L_{rank} . The classification loss is formulated as a cross-entropy loss to accurately predict whether each pose has an RMSD below 2 Å. Furthermore, we adopt a pairwise ranking loss inspired by InstructGPT (Ouyang et al., 2022). For each batch, samples are copied N_{copy} times, generating $\binom{N_{copy}}{2}$ for each protein-ligand complex. We train on all $\binom{N_{copy}}{2}$ comparisons from each complex as a single batch element. According to InstructGPT, this method is computationally more efficient and reduces the likelihood of overfitting. The ranking loss is formally defined as follows:

$$L_{rank} = -\frac{1}{\binom{N_{copy}}{2}} E_{(R_+, R_-) \sim D} [\log (\sigma (f_\theta (R_+) - f_\theta (R_-)))], \quad (3)$$

where $f_\theta(R)$ is the scalar score predicted by the confidence model for conformation R , R_+ is the preferred conformation with lower RMSD compared to R_- , and D is the dataset of comparison sets.

⁴<https://github.com/DeepGraphLearning/torchdrug>

⁵<https://graph-tool.skewed.de/>

⁶<https://networkx.org>

In the implementation, each GPU batch consists of $N_{sample} = 1$ samples, which are then duplicated $N_{copy} = 8$ times. Following model forward propagation, each sample yields N_{copy} predicted structures. These structures are subsequently ranked according to their computed RMSD values, which are also utilized to calculate the classification loss L_{cls} . The total loss for the confidence model, denoted as L_{conf} , is the sum of the classification loss and the ranking loss: $L_{conf} = L_{cls} + L_{rank}$.

C. Training and Inference

MLP Configuration. All multilayer perceptrons (MLPs) implemented in FABind+ consist of a Layer Normalization, followed by two linear transformations with ReLU activations. An additional ReLU activation is applied after the final linear transformation if the output of the MLP is an embedding. To regulate the parameters of FABind+, the MLP hidden scale is set to 1, indicating that the MLP’s hidden size is the same as the input embedding dimension. On the other hand, in the confidence model, the MLP hidden scale is increased to 4 to maximize the model capacity.

Training Details for FABind+. Our FABind+ models are trained on eight NVIDIA Tesla V100 GPUs for 1500 epochs. We use Adam (Kingma & Ba, 2014) as the optimizer, and set the hyperparameter ϵ to $1e-8$ and (β_1, β_2) to $(0.9, 0.999)$ with no weight decay. The peak learning rate is set to $5e-5$ with a 15-epoch warmup stage followed by a linear decay learning rate scheduler. The dropout probability and total batch size are set to 0.1 and 16.

We list the detailed hyperparameter search configuration in Table 4. For dynamic radius prediction, we try to aggregate embeddings from different components (protein embedding, ligand embedding, or both) and find that aggregating ligand embedding yields superior performance. Additive (ADD) and multiplicative (MUL) radius buffers are also tested. They have comparable performance, but the latter induces greater training instability; thus, we choose the additive buffer. The loss weights for each training objective prove to be sensitive in the multitask learning framework. Additionally, introducing noise to the three dimensions of the predicted binding site center during the training phase enhances model robustness significantly. Noises within a range of 0.0 to 5.0 Å are sampled each time.

Table 4. The hyperparameter options we searched through for FABind+. The final parameters are marked in **bold**.

PARAMETER	SEARCH SPACE
<i>Model Config</i>	
RADIUS PREDICTION FROM	PROTEIN, LIGAND, BOTH
RADIUS BUFFER	ADD (5Å, 10Å), MUL ($\times 1.5, \times 2.0$)
MLP HIDDEN SCALE	1, 2, 4
DROPOUT	0.0, 0.1
USING LAYERNORM	YES, NO
NON LINEARITIES	RELU
<i>Training Config</i>	
LEARNING RATES	1E-4, 7E-5, 5E-5 , 3E-5
BATCH SIZE	8, 16
POCKET LOSS WEIGHT (CLS-REG-RADIUS)	{0.5, 1.0 }-{0.05, 0.2}-{0.01, 0.05 , 0.2, 0.4}
DOCKING LOSS WEIGHT (COORD-DISTMAP-DISTILL)	{1.0, 1.5 , 2.0}-{0.0, 1.0 , 2.0}-{0.0, 1.0 }
NOISE FOR PREDICTED POCKETS	RANGE(0, 5)

Table 5. The hyperparameter options we searched through for confidence model. The final parameters are marked in **bold**.

PARAMETER	SEARCH SPACE
<i>Model Config</i>	
MODEL BACKBONE	MLP, STACKED MLP, NODE MLP, FABIND LAYER
MLP HIDDEN SCALE	1, 4
<i>Training Config</i>	
TRAINING OBJECTIVE	CLASSIFICATION, RANKING, BOTH
LEARNING RATES	1E-3, 1E-4 , 1E-5
NUM OF SAMPLES PER BATCH	8, 16
NUM OF COPIES	8

Training Details for Confidence Model. The computational overhead for confidence model training is notably lower, requiring 15 epochs of training on eight NVIDIA Tesla V100 GPUs. The detailed hyperparameter options are listed in Table 5. We evaluate various model backbones for feature extraction, namely MLP, Stacked MLP, Node MLP, and FABind layer. Stacked MLP refers to the configuration where two previously described MLPs are stacked, thus expanding two sub-layers to four. Node MLP denotes an additional MLP transformation applied to node embeddings prior to their aggregation (sum). Subsequent to aggregation, another MLP updates the features for the output. Incorporating an additional FABind layer results in the highest parameter count. However, we observe limited benefit in enhancing the confidence model’s capability. This underscores that generalization is crucial for the efficacy of the confidence model.

During training, our confidence model can generate training examples on-the-fly, in contrast to the approach in DiffDock (Corso et al., 2023b), which requires offline storage of sampled structures. This difference arises because DiffDock treats the scoring and confidence models as separate models, whereas our method integrates them into a single model. With the sampling mode on, the confidence model can directly utilize samples generated by FABind+. Consequently, an MLP-based backbone suffices due to the robust feature extraction capabilities of the preceding FABind+.

D. Further Analysis

D.1. Pocket Prediction Study

In reference to Figure 3, we further compare the pocket prediction performance between FABind and FABind+ on the test set, as depicted in Figure 9. “Max Distance” represents the distance between the predicted pocket center and the farthest ground truth ligand atom. This offers an approximation of the pocket size required to encompass the ligand based on the predicted pocket center. From this Figure 9, we can see that FABind+ shows better performance with a lower RMSD score than FABind across samples with different max distances, which demonstrates the effectiveness of our enhanced designs. For those samples with a large max distance, our method’s precise pocket prediction and dynamic radius prediction capabilities enable more accurate prediction.

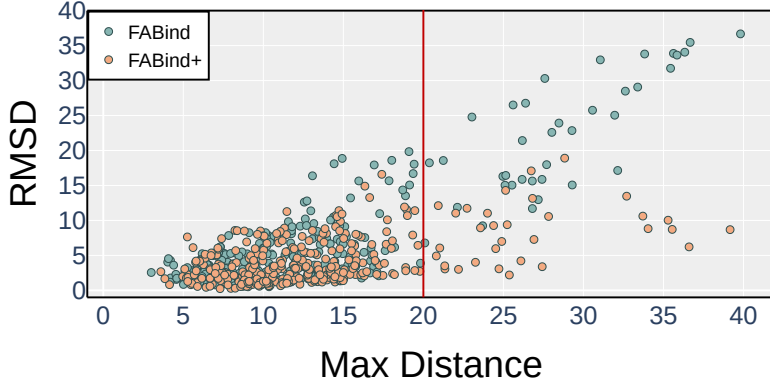


Figure 9. Analysis of pocket prediction and the predicted ligand RMSD. “Max Distance” is the distance between the predicted pocket center and the farthest ground truth ligand atom.

D.2. Ablation Study

Model Size and Inference Speed. We conduct comprehensive studies on the relationship between model size, performance, and inference speed, as illustrated in Figure 10. The x-axis denotes inference speed, while the y-axis represents performance, specifically the fraction of RMSD below 2Å. The size of the circles in the figure correlates with the number of parameters in the model. This figure suggests that larger models typically offer better performance but at the expense of reduced inference speed. Notably, the largest model setting does not yield improved results, potentially due to the need for meticulous hyperparameter tuning to unlock optimal performance.

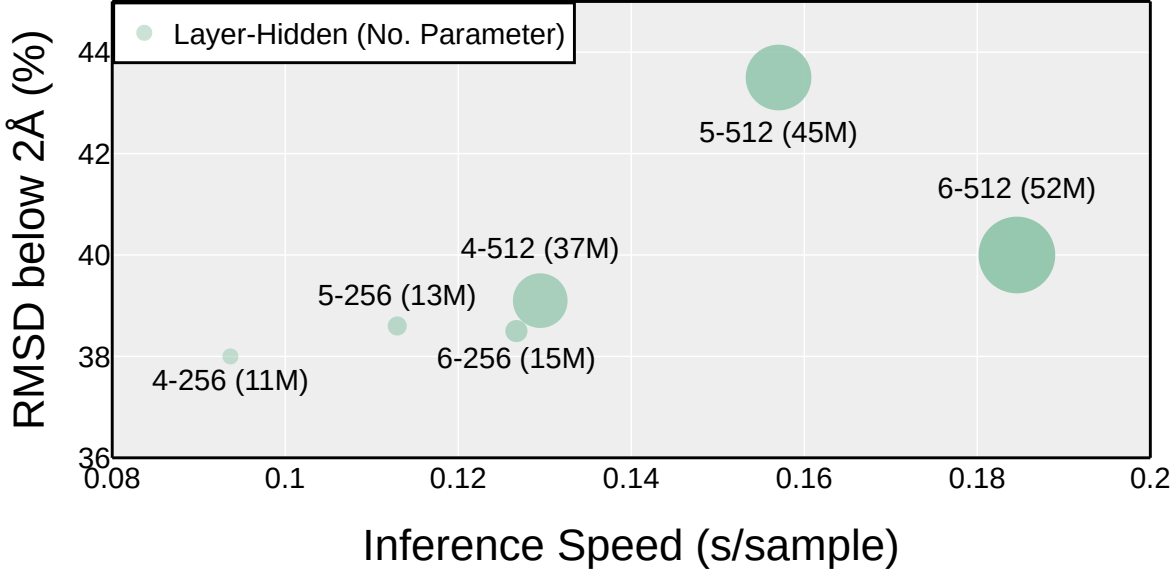


Figure 10. Ablation of model size.

Ablations for Regression FABind+. To transition from FABind to a regression-based method, we implemented several enhancements depicted in Figure 14. The introduction of radius prediction and permutation loss contributed to performance increases of 3.0% and 2.1%, respectively. A thorough hyperparameter search further unlocked the model’s capabilities, yielding an additional 2.1% improvement. Given the presence of six loss functions in our framework, fine-tuning the weights assigned to each loss function had a significant impact on the results. Moreover, we discovered that simply increasing the number of layers could also lead to a performance gain. However, it is important to note that deeper architectures require a more careful parameter study.

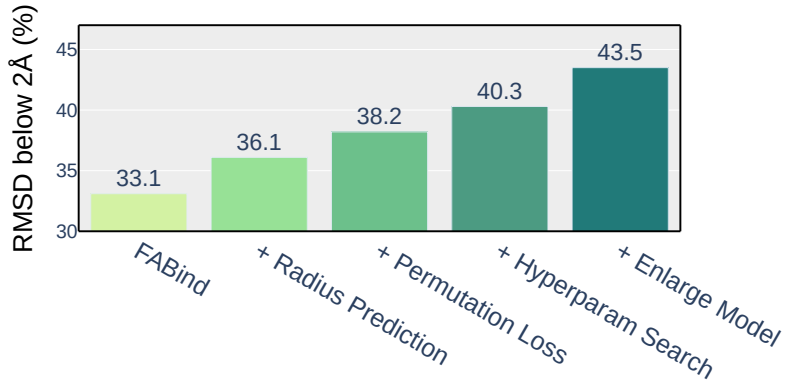


Figure 11. Performance gain from FABind to FABind+.

Ablations for Sampling FABind+. For the sampling version, we present a scaling curve in Figure 12 to illustrates how performance changes for different ablations. Here, “FABind+” represents our sampling-based model. “No Dropout” refers to our model operating without dropout sampling during both training and inference phases, whereas “No Clust” indicates the absence of pocket clustering.

This figure underscores the importance of each design element in achieving optimal performance. Specifically, removing pocket clustering leads to a slight drop in performance, as it hinders the ability to capture multiple binding sites. The lack of dropout sampling means that diversity relies entirely on pocket clustering. However, given the limited number of pockets, the orange dashed line in the graph exhibits only a minimal increase with sample size.

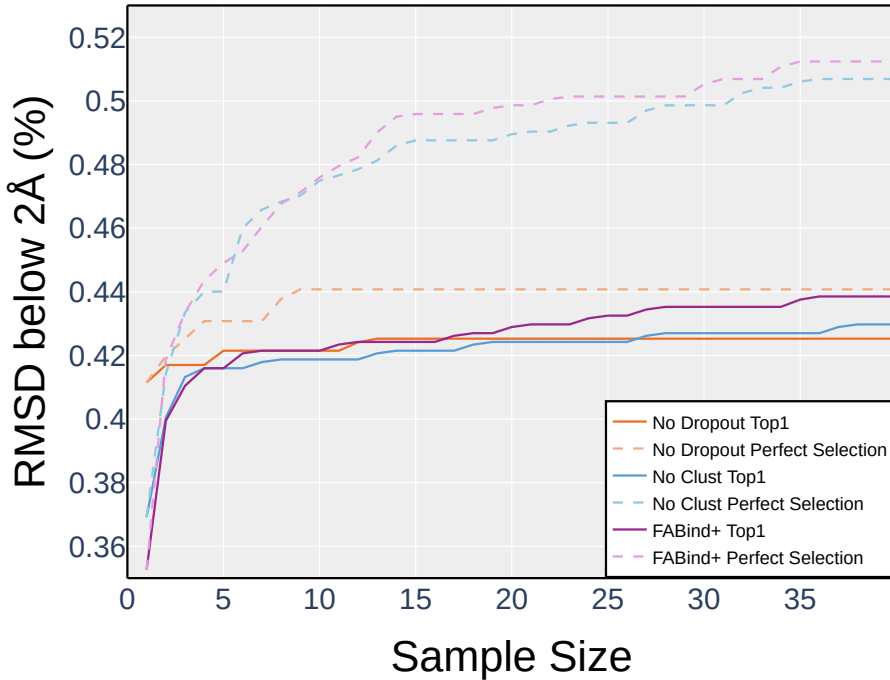


Figure 12. Ablation analysis for the sampling version.

E. Visualizations

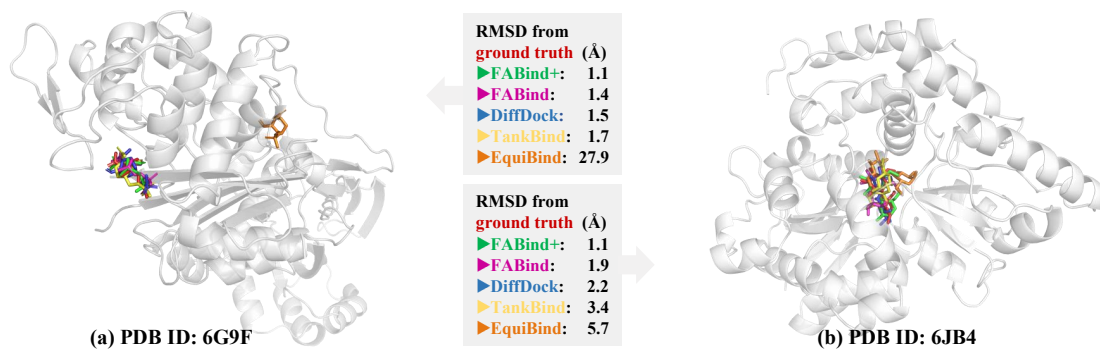


Figure 13. Case studies for Regression-based FABind+. Structures predicted by FABind+ (green), FABind (magentas), DiffDock (blue), TankBind (yellow) and EquiBind (orange) are placed together with the protein target, with the RMSD to the ground truth (red) reported. These comparisons underscore the capability of FABind+ for accurate prediction.

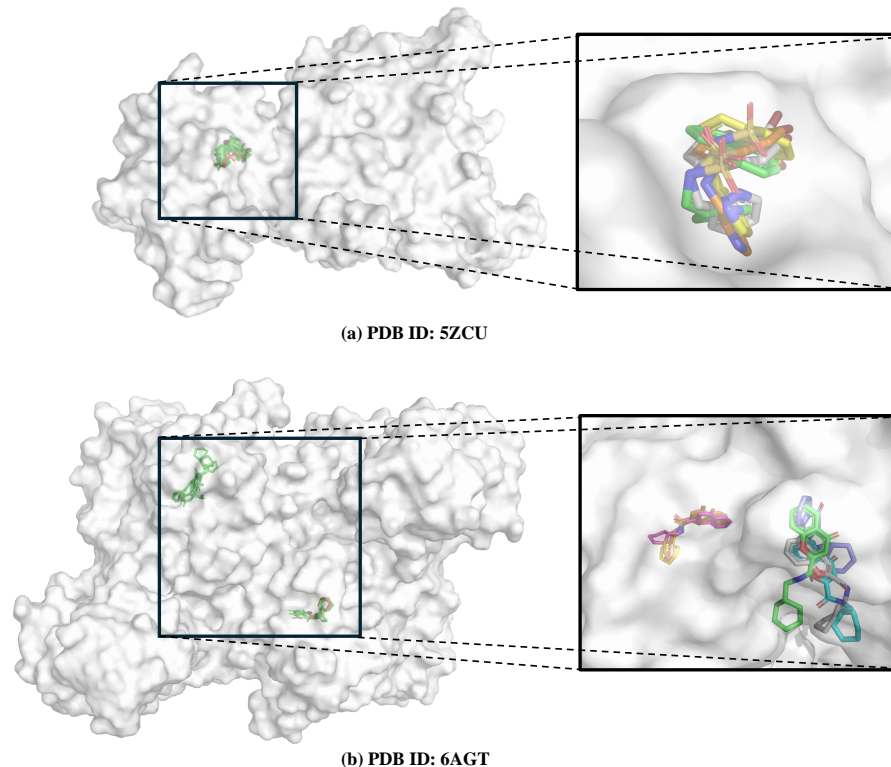


Figure 14. Sampling diversity and quality with FABind+. On the left, sampled structures (green) alongside the ground truth (red) are depicted; on the right, a closer view of the sampled structures is provided, each colored randomly for distinction. (a) In the case of complex 5ZCU, which features a single binding site, FABind+ successfully generates a variety of conformations that are centered around the ground truth. (b) For complex 6AGT, characterized by multiple pockets, FABind+ not only identifies these pockets but also generates diverse structures within each pocket.